Published in final edited form as:
Cancer Cell. 2009 May 5; 15(5): 389–401. doi:10.1016/j.ccr.2009.03.004.

CDK inhibitor p18^{INK4c} is a downstream target of GATA3 and restrains mammary luminal progenitor cell proliferation and tumorigenesis

Xin-Hai Pei[1,6], **Feng Bai**[1,6], **Matthew D. Smith**[1], **Jerry Usary**[1], **Cheng Fan**[1], **Sung-Yun Pai**[5], **I-Cheng Ho**[5], **Charles M. Perou**[1,2,4], and **Yue Xiong**[1,3,*]

1 *Lineberger Comprehensive Cancer Center, University of North Carolina at Chapel Hill, Chapel Hill, NC 27599-7295*

2 *Department of Genetics, University of North Carolina at Chapel Hill, Chapel Hill, NC 27599-7295*

3 *Department of Biochemistry and Biophysics, University of North Carolina at Chapel Hill, Chapel Hill, NC 27599-7295*

4 *Department of Pathology and Laboratory Medicine, University of North Carolina at Chapel Hill, Chapel Hill, NC 27599-7295*

5 *Department of Pediatric Hematology-Oncology, Dana-Farber Cancer Institute and Children's Hospital, Harvard Medical School, Boston, MA 02115*

SUMMARY

Mammary epithelia are composed of luminal and myoepithelial/basal cells whose neoplastic transformations lead to distinct types of breast cancers with diverse clinical features. We report that mice deficient for the CDK4/6 inhibitor p18^{Ink4c} spontaneously develop ER-positive luminal tumors at a high penetrance. *Ink4c* deletion stimulates luminal progenitor cell proliferation at pubertal age and maintains an expanded luminal progenitor cell population throughout life. We demonstrate that GATA3 binds to and represses *INK4C* transcription. In human breast cancers, low *INK4C* and high *GATA3* expressions are simultaneously observed in luminal A type tumors and predict a favorable patient outcome. Hence, p18^{INK4C} is a downstream target of GATA3, constrains luminal progenitor cell expansion and suppresses luminal tumorigenesis in the mammary gland.

SIGNIFICANCE—Breast cancer is heterogenous with tumors pathologically distinct and diverse in their responsiveness to treatment. We show that the CDK inhibitor p18^{INK4c} gene is repressed by GATA3, a transcription factor specifying mammary luminal cell fate, and that low *INK4C* and high *GATA3* expressions are associated with human luminal A type tumors and with better patient survival. p18^{Ink4c} null mice have an expanded luminal progenitors at a young age and throughout life and develop ER^{+} luminal tumors at high penetrance. These results identify the escape of luminal progenitors from quiescence as a rate-limiting step for initiation of mammary luminal tumors. The *Ink4c*-null mouse represents a unique model for study and for developing therapeutic strategies to treat luminal tumors.

*Correspondence: E-mail: yxiong@email.unc.edu.
6These authors contributed equally

Keywords

INK4c; *GATA3*; luminal progenitor; stem cell; breast cancer; tumor suppression

Introduction

Mammary epithelia are comprised of two major epithelial cell types: ductal and alveolar luminal cells, constituting the inner layer of ducts and the lobuloalveolar units, respectively; and a basal layer of myoepithelial cells surrounding the luminal cells. Both epithelial cell types are believed to originate from a common multipotential stem cell (Shackleton et al., 2006; Stingl et al., 2006). Histopathologically, breast cancer can be divided into two major types: luminal tumors that account for the majority of breast cancer cases (70–80%) and are typically estrogen receptor (ER) positive; and basal-like breast cancers that have high histological grades and mitotic indices, are ER-negative, and are associated with a poor prognosis (Althuis et al., 2004). Gene expression profiling analyses have further categorized human breast tumors into several intrinsic subtypes that correlate with tumor biology and are prognostic and predictive for patient outcomes (Hu et al., 2006; Perou et al., 2000; Sorlie et al., 2003). The genetic, cellular, and biochemical mechanisms controlling lineage commitment and maturation in the mammary gland bear clinical significance, as different types of breast tumors possess different outcomes and are diverse in their responsiveness to treatment but remain to be defined. The cellular origin of breast cancer and how its various subtypes arise are not fully understood, and appropriate animal models for studying this disease are still needed.

p18^{Ink4c} (referred to as p18 hereafter) is a member of the mammalian INK4 family that inhibits CDK4 and CDK6, whose activation by mitogen-induced D-type cyclins leads to phosphorylation and functional inactivation of RB, p107, and p130. Functional inactivation of this pathway is a common event in the development of most types of cancer (Sherr, 1996). p18 is a haploinsufficient tumor suppressor in mice whose deletion promotes the development of various tumors, including lymphoma, medulloblastoma, glioblastoma, and tumors of neuroendocrine organs, lung, and prostate (Bai et al., 2003; Bai et al., 2006; Franklin et al., 1998; Latres et al., 2000; Pei et al., 2007; Uziel et al., 2005). Deletion or reduced expression of the *p18* gene has also been observed at high frequency in different types of human cancer.

Three lines of evidence suggest a potential function of *p18* in suppressing mammary tumors. First, the *cyclin D1* gene, located on human chromosome 11q13 and a functional antagonist of p18, is amplified in a substantial portion of human breast cancer [reviewed in (Ormandy et al., 2003)]. Transgenic expression of *MMTV-cyclin D1* promotes mammary tumor development (Wang et al., 1994). Second, deletion in mice of *cyclin D1* or *CDK4*, the target of p18, conversely retards mammary gland development and prevents MMTV-oncogene induced mammary cancer (Fantl et al., 1995; Sicinski et al., 1995; Yu et al., 2001; Yu et al., 2006). Lastly, female *p18* null mice (in BL/6 background) display mammary gland hyperplasia with ectasia in their galactophor ducts (Latres et al., 2000 and our unpublished observation). We carried out this study to determine the function and mechanism of *p18* in suppressing mammary tumorigenesis.

Results

p18$^{-/-}$ mice develop predominantly ERα positive luminal mammary tumors

To determine the function of *p18* in mammary tumor suppression, we introduced *p18*$^{-/-}$ into the Balb/c strain, which is known to be susceptible to mammary tumor development and is widely used for such study, by backcross (Ponnaiya et al., 1997; Ullrich et al., 1996). The tumor spectrum, incidence and onset time of many tissues, including pituitary, thyroid, testis,

pancreas, and lung, increased in the Balb/c background compared with the BL/6 background (data not shown). The most striking phenotype in Balb/c-*p18* mice was mammary gland tumors, as the mammary tumor-free survival was reduced from a mean age of 27.3 months in wild-types (WT), to 20.9 months in $p18^{+/-}$, and to 15.4 months in $p18^{-/-}$ (Figure 1A).

Mammary tumors developed in Balb/c-$p18^{-/-}$ mice at a very high incidence, including 23% (N=13) of females examined less than one year of age and 88% (N=17, including 1 male) between one year and 20 months (Figure 1B). Most mammary tumors from $p18^{-/-}$ and $p18^{+/-}$ mice were preinvasive carcinomas, such as ductal carcinoma in situ (DCIS), and exhibited papillary, cribriform. and cystic characteristics with low and intermediate nuclear grades (Figure 1C). Only two of 18 (11%) $p18^{-/-}$ mammary tumors were invasive ductal carcinoma (IDC), and one of them metastasized to the lung.

Normal breast ducts contain two types of epithelial cells: luminal cells that are round or polygonal and line the inner ductal lumen; and basal/myoepithelial cells that are elongated and contact the basement membrane but never contact the lumen. Luminal and basal/myoepithelial cells can also be distinguished by their different cytokeratin (CK) expression patterns. The majority of luminal cells express CK7, 8, 18, 19, and 20, while basal/myoepithelial cells typically express CK5, 13, 14, and 17. $p18^{-/-}$ mammary carcinomas, most of which retained an organized gland and duct structure, stained strongly and uniformly for CK8 but not CK5, indicating that they predominantly contain luminal epithelial cells (Figure 1D).

Most (13 out of 15, 87%) $p18^{-/-}$ mammary tumors examined were positive for estrogen receptor alpha (ERα). The percentages of ERα positive cells varied among individual $p18^{-/-}$ mammary tumors, from as low as 2–5% in six tumors, to more than 20% in the other nine, indicating heterogeneity and potentially different stages of tumor development. ERα positive cells were frequently detected in $p18^{-/-}$ mammary tumors, where tumors were well-differentiated and still retained an overall normal architecture of mammary glands (Figure 1E, left and middle), or when poorly-differentiated tumors were investigated (Figure 1E, right). When compared with 13 different murine mammary tumor models (Herschkowitz et al., 2007), $p18^{-/-}$ mammary tumors express the highest level of ER (data not shown). It should be pointed out, however, that most mammary tumors developed in $p18^{-/-}$ mice are DCIS, with only 11% IDC or metastatic tumors, whereas mammary tumors developed in other murine models are mostly invasive carcinoma. It remains to be determined whether the difference in ER expression between $p18^{-/-}$ tumors and tumors of 13 other models reflects different stages in tumor progression or inherent differences in tumor biology. Together, these results suggest that *p18* plays an important role to suppress the development of ERα-positive luminal mammary tumors in mice.

p18 deficiency stimulates proliferation and Rb protein phosphorylation in luminal cells

We determined cell proliferation in mammary tumors developed in $p18^{-/-}$ mice (>14 months of age) by examining both the proliferation marker Ki67 (Figure 2A) and the mitotic marker phosphorylated histone H3 (data not shown). Both analyses revealed that there was active cell proliferation in $p18^{-/-}$ mammary tumors compared with mammary tissues derived from age-matched $p18^{+/-}$ or WT mice. As determined microscopically by their inner localization in the mammary glands, a majority of proliferating cells in $p18^{-/-}$ mammary tumors were luminal cells.

We then determined mammary epithelial proliferation by pulse-labeling 9-month-old virgin littermate WT and $p18^{-/-}$ mice with BrdU. At this age, most $p18^{-/-}$ mammaries exhibit either normal appearance or hyperplasia and retain relatively normal architecture of mammary glands but not yet developing tumors. There was very little cell proliferation in WT ductal epithelium, and as expected, BrdU incorporation was barely detectable (Figure 2B, note that green

fluorescence outside the glands does not correspond to individual cells and was likely caused by non-specific staining). In contrast, BrdU-positive cells in littermate $p18^{-/-}$ ductal epithelium were substantially increased. Microscopic examination of four independent mammary glands from three different mice of each genotype revealed a 3.8-fold increase of BrdU positive cells in $p18^{-/-}$ mammary glands (6.4% ± 2.3%) than in WT glands (1.7% ± 0.7%, Figure 2B). Most $p18^{-/-}$ ducts/glands contained more than two BrdU+ cells, and nearly all BrdU+ cells were also positive to CK8 staining, indicating that the majority of BrdU+ cells were luminal epithelia. Only a few BrdU-positive cells co-expressed CK5, a marker for myoepithelial cells (data not shown).

At eight weeks of age, mammary ducts branch with active epithelial cell proliferation, including both luminal and myoepithelial cells, and no lesions were detected in $p18^{-/-}$ mammaries as confirmed by parallel H&E staining (data not shown). *p18* deficiency resulted in a 2.5-fold increase of BrdU positive cells in mammary epithelium, most of which were luminal-like epithelial cells (Figure 2C). Finally, we directly examined the status of Ser608 phosphorylation of Rb protein, the site that is preferentially phosphorylated by p18's targets CDK4 and CDK6 (Schmitz et al., 2004; Zarkowska et al., 1997). A visible and consistent increase of pRb-Ser608 phosphorylation, both in the intensity and number of positive cells, was seen in normal $p18^{-/-}$ mammary epithelia (11.2 ± 1.8% in wt to 23.5 ± 3.8% in $p18^{-/-}$) and $p18^{-/-}$ tumors (34.5 ± 5.7%, Figure 2D), supporting the activation of CDK4 and/or CDK6. Most Rb-Ser608 positive cells were luminal cells. Taken together, these results demonstrate that *p18* deficiency stimulates CDK4 and/or CDK6 activity towards the Rb protein in luminal epithelial cells, increasing their proliferation in a cell autonomous manner at an early age prior to the development of any detectable preneoplastic lesion. Loss of *p18* also maintains luminal cells at a hyperproliferative state throughout adulthood, during which time $p18^{-/-}$ luminal cells progressively develop from hyperplasia to tumor.

Loss of *p18* increases label-retaining luminal epithelial cells

We explored the possibility that *p18* loss stimulates mammary stem and/or luminal progenitor cell proliferation. One unique feature of stem/progenitor cells is their slow rate of proliferation. As a result, the BrdU label incorporated during a long period of pulse labeling can be retained after a long period of chase by the stem/progenitor cells but are continuously diluted in other somatic cells by each cell cycle. Label-retaining cells (LRCs) have been demonstrated to be enriched in both mammary stem and progenitor cells (Shackleton et al., 2006; Smith, 2005; Welm et al., 2002). We injected BrdU into pubertal littermates twice a day consecutively for seven days and determined the LRCs after short (1 day) and long (37 days) chase. At day 1 of chase, more than half of the epithelial cells were BrdU positive in both WT (51.7% ± 6.8%) and $p18^{-/-}$ mammaries (55.3% ± 8.1%) (Figure 3A). After 37 days of chase, BrdU positive LRCs were only sparsely detected in the WT mammaries but were notably increased in $p18^{-/-}$ mammaries (Figure 3B). Microscopic examination of 12 mammary glands from three mice of each genotype revealed a 1.6-fold increase of LRCs in $p18^{-/-}$ mammary glands (14.5% ± 1.8%) over WT glands (9.1% ± 1.3%).

Most LRCs in both WT and $p18^{-/-}$ mammaries were round or polygonal, located in the inner layer of the duct, and made contact with the ductal lumen, indicative of luminal epithelium. To confirm this, we stained mammary sections with CK8 and CK5 and determined that indeed, most WT (7.3% ± 1.4% of total mammary epithelium and 80.2% of total LRC) and $p18^{-/-}$ LRCs (12.04% ± 1.7% of total mammary epithelium and 83% of total LRC) were positive for CK8 (Figure 3B). Notably, the CK8-positive LRCs, which are likely enriched for luminal progenitor cells, were increased by 1.7-fold by *p18* loss, from 7.3% of total epithelial cells in WT mammaries to 12% in $p18^{-/-}$ mammaries (Figure 3B).

Loss of *p18* increases cells with morphologic features of luminal progenitors

Previously, Smith and colleagues combined light and electronic microscopic analyses of the mammaries from different mammals and defined five histologically distinct epithelial cell populations based on the cell size and nuclear and cytoplasmic staining characteristics: small light cell (SLC), undifferentiated large light cell (ULLC), differentiated large light cell (DLLC), large dark cell (LDC), and myoepithelial cell (MYO) (Chepko et al., 2005; Smith and Medina, 1988). Both small and large light cells appear to be division-competent, based on their condensed chromosomes and capability to undergo mitosis in explant culture. Combined with the characterization of the cytoplasmic organelle differentiation and localization in the glands, these features led to the proposal that SLCs represent a population enriched for mammary stem cells that divide and differentiate progressively into ULLC, likely corresponding to the luminal progenitors, and then to DLLC, before terminal differentiation into a bulk population of mature luminal cells (LDCs).

To determine the division-competency of these structurally defined cell populations and their label retaining ability, we took immunostained sections from the label retaining assay (37-day chase), re-stained them with H&E, and matched 793 cells from WT and 946 cells from *p18*$^{-/-}$ mammaries from two stainings by side-by-side microscopic comparison (Figure 3C and Table S1). Of these matched cells, 70 from WT and 150 from *p18*$^{-/-}$ mammaries were LRCs and close to half, 44% in WT and 48% in *p18*$^{-/-}$ mammary, respectively, corresponded to ULLCs. The remaining LRCs were similarly distributed among SLCs, DLLCs, LDCs, and MYOs (Table S1). This result indicates that ULLCs represent the majority of LRCs, providing functional support to the histologically defined notion that ULLCs represent a progenitor-enriched mammary epithelial cell population.

We next microscopically examined more than 20 ducts and lobules from each animal of both genotypes between two and three months of age, and counted at least three lobules and one duct per animal (Figure S1). Of five major populations, the ULLC population was significantly increased from 16.5% in ducts and 19% in lobules of WT mammaries, to 28.1% and 25% in *p18*$^{-/-}$ ducts and lobules, respectively, and led to a 50% overall increase of ULLCs from WT (17.6%) to *p18*$^{-/-}$ (26.5%) mammaries (Figure 3D, and Figure S1). The SLC population was very small (less than 3%) and partially overlapped with myoepithelial cells in their localization, making it difficult to determine whether *p18* deletion also affects the size of the putative mammary stem cell population. There is no significant difference in relative distribution of the other three populations, as well as cells of unknown (UK) origin, between WT and *p18*$^{-/-}$ mammaries (Figure S1). These results demonstrate that luminal progenitor-enriched ULLCs are the major cell population affected by the loss of *p18* at an early age, prior to tumor development.

p18 deficiency expands and maintains the luminal progenitor-enriched cell population

To corroborate the finding that loss of *p18* expands luminal progenitor cells, we dissected mammary glands from 6–8 week mice and analyzed them by flow-cytometry. After exclusion of lymphocytes (SSC low), dead cells (7AAD positive), hematopoietic cells ($CD45^+TER119^+$), and endothelial cells ($CD31^+$), the expression profile for CD24 and CD29 was determined (Figure S2A). The $CD29^{lo}CD24^+$ population, that is enriched with progenitors and have a luminal cell fate under lactogenic condition (Asselin-Labat et al., 2007; Shackleton et al., 2006; Sleeman et al., 2007), was increased by 1.5-fold in *p18*$^{-/-}$ mammaries compared to WT littermates in Balb/C (42.3 ± 2.5% vs 27.9 ± 3.7%, Figure 4A) and 1.4-fold in BL/6 (51% vs 35.9%, Figure S2B) backgrounds at pubertal age (6–8 week). The $CD29^{lo}CD24^+$ cells were very similar between *p16*$^{-/-}$ and *p16*$^{+/-}$ (26.52% vs. 25.83%, data not shown), supporting a specific role of *p18* in controlling luminal progenitor cell proliferation in pubertal mice. The $CD29^{lo}CD24^+$ cell population was similarly increased in postpubertal (10–12 week) *p18*$^{-/-}$

mammaries (42.7 ± 4.0% vs 34.1 ± 2.6%, Figure 4A), and remained high late in life in *p18*$^{-/-}$ mice, 48.3% at 9 months of age and 37.8% (in hyperplasic tissues) or 42.1% (in tumorigenic tissues) at 14 months of age, and both were higher than WT littermates (41% and 34% at 9 and 14 months of age, respectively). These data suggest that *p18* loss results in a continuous increase of luminal progenitor-enriched CD29^{lo}CD24^{+} cell population during aging and development.

CD49f (α6 integrin) is expressed in human mammary colony forming cells (Ma-CFC) enriched for luminal progenitor cells and has also been used in combination with CD24 to identify mouse Ma-CFCs and stem cells (Stingl et al., 2001, Stingl, 2006). After exclusion of lymphocytes and dead, hematopoietic, and endothelial cells, we determined that the CD24^{high}CD49f^{low} population was significantly increased in *p18*$^{-/-}$ mammaries compared with WT littlemates by 1.8-fold in Balb/c (6 wk, 7.9% vs 4.2%, Figure 4B) and 1.7-fold in BL6 (12 wk, 6.6% vs 3.8%, Figure S2D) backgrounds. The CD24^{high}CD49f^{high} population enriched for mammary stem cells, on the other hand, did not appear to be significantly affected by *p18* loss (3.6% vs. 3.2%, Figure 4B). The CD24^{high}CD49f^{low} population in *p18*$^{-/-}$ mammary at 11 months of age also remained higher than in WT littermate mammaries (5.5% vs 4.0%, Figure S2E). These results further support the function of *p18* in constraining luminal progenitor expansion.

CD24^{+} mammary epithelial cells are enriched for luminal cells and can be further separated into two distinct populations based on the expression of either Sca1 or prominin-1, which almost completely overlap: a CD24^{+}Sca1^{-} or CD24^{+}prominin-1^{-} population that is enriched (>40%) for colony-forming cells (CFCs, i.e. luminal progenitor cells); and a CD24^{+}Sca1^{+} or CD24^{+}prominin-1^{+} population that is enriched (>80%) for cells expressing genes involved in sensing systemic hormones such as ERα, progesterone receptor, and prolactin receptor and contains little stem cell activity (Sleeman et al., 2006; Sleeman et al., 2007). Consistent with the expansion of the CD29^{lo}CD24^{+} cell population, the CD24^{+}Sca1^{-} population was also higher in *p18*$^{-/-}$ mice than in littermate WT mice at postpubertal age (28.3% vs.23.3%) and maintained at a higher level later in life; 59% in *p18*$^{-/-}$ vs. 50% in WT mice at 9 months of age and 57% in *p18*$^{-/-}$ vs. 41.7% in *p18*$^{+/-}$ mice at 14.5 months of age (Figure 4C). Similar results, that *p18* deficiency increased both CD24^{+}Sca1^{-} (14% vs. 9%) and CD24^{+}Sca1^{+} populations (39% vs. 25%) when compared with WT littermates, were also obtained in BL/6 mice (Figure S2C), indicating that the function of *p18* in constraining luminal cells is not strain-dependent.

To directly demonstrate that the proliferation of luminal progenitor cell populations is increased in *p18*$^{-/-}$ pubertal mice, we isolated mammary epithelial cells and stained them with CD24 and intracellularly with the proliferation marker Ki67 after depletion for lymphocytes and Lin + cells. The CD24^{+}Ki67^{high} population was increased from 29.3% in WT mammaries to 43.1% in *p18*$^{-/-}$ mammaries (Figure 4D), providing further evidence to conclude that *p18* loss initiates the expansion of a luminal progenitor-enriched cell population.

p18 constrains luminal progenitor cell proliferation in a cell autonomous manner

We next determined the function of *p18* in constraining luminal progenitor cell proliferation using three different in vitro systems: 3D Matrigel, mammosphere, and colony formation assays. The Matrigel assay showed that mammary cells derived from *p18*$^{-/-}$ mice exhibited a substantial increase of proliferation and that the majority of BrdU positive cells were luminal (Figure 5A), demonstrating that the increased proliferation of luminal *c*ells in *p18*$^{-/-}$ mice is cell autonomous. Mammary stem/progenitors propagated in nonadherent culture in vitro form mammospheres and are able to differentiate into both luminal and basal/myoepithelial lineages (Dontu et al., 2003). Cells derived from *p18*$^{-/-}$ mammaries showed an increase in primary mammosphere forming activity, 32.8 ± 5.1 spheres/20,000 cells, than WT cells, 26.3 ± 3.4 spheres/20,000 cells (p=0.027, paired t-test, Figure 5B), indicating increased stem or progenitor

cell function resulting from *p18* loss. Most WT spheres were 70–100 μm in size with 10–20% larger than 100 μm, whereas most $p18^{-/-}$ spheres were 80–120 μm in size with 10–20% spheres larger than 120 μm (Figure 5B). The average size of $p18^{-/-}$ spheres (118 ± 38 μm) was significantly larger than WT spheres (92 ± 24 μm, p=0.017, paired t-test, Figure 5B), further supporting the conclusion that *p18* loss increases the proliferative potential of mammary progenitor cells. To examine their differentiation potential, we induced individual mammospheres to differentiate. After four days of culture in gelatin-coated dish, most cells in the spheres were attached, differentiated, and migrated out of the center. Immunostaining identified $CK8^+$ and $CK5^+$ cells in both WT and $p18^{-/-}$ spheres (Figure S3), confirming that the spheres were capable of differentiating into both luminal and basal/myoepithelial lineages and that *p18* deficiency did not affect the differentiation potential of the mammosphere.

We then compared the colony-forming capacity of WT and $p18^{-/-}$ mammary epithelial cells (MECs) in Matrigel and scored both spherical and flat colonies. For scoring spherical colonies, we divided them into >50 μm and >100 μm groups and found that $p18^{-/-}$ MECs formed more spherical colonies in both groups, averaging 10.8 colonies >100 μm or 9.5 colonies >50 μm per 1,000 MECs seeded, compared to WT or heterozygous MECs that formed on average 6.8 colonies >100 μm or 4.5 colonies >50 μm per 1,000 MECs seeded (Figure 5C). The $p18^{-/-}$ MECs also appeared to form more flat colonies in both size groups, but the limited number of flat colonies formed by both WT and $p18^{-/-}$ MECs prevented us from making a statistically significant determination (Figure 5C). Because we used MECs in these FACS and colony-formation assays, we cannot exclude the possibility that *p18* may also have a function in regulating stroma cells in vivo, which could contribute to the control of luminal progenitor cell expansion. Almost all spherical colonies generated from either WT or $p18^{-/-}$ MECs, including both acini with or without lumen, stained strongly for CK8, with varying degrees of CK5 staining (Figure S4A). Staining of colonies after dissolving Matrigel revealed two distinct groups of colonies: one containing cells in the center that were strongly stained for CK8 and a few outer layer cells that were stained positively for CK5 (Figure S4B, left panels); and one comprised uniformly of $CK8^+$ cells throughout the colony (right panels).

To obtain a quantitative assessment, we generated more colonies by seeding a high density of unsorted mammary cells on Matrigel (20-fold more than clonal density). Flat colonies were difficult to identify accurately due to their high density and were not counted. $p18^{-/-}$ mammary cells formed significantly more spherical colonies in both >50 μm and >100 μm size groups and slightly more colonies larger than 200 μm compared with WT littermate mammary cells (Figure S4C). Most spherical colonies stained strongly for CK8 with varying degrees of CK5 staining.

Considering that serum-free culture conditions favor luminal cell proliferation, which may cause an underestimation of the myoepithelial cells, we divided the spherical colonies into two groups: ‘basal colonies’ (CK8+ and more than 50% CK5+ cells) and ‘luminal colonies’ (CK8 + and less than 50% CK5+ cells) (Figure 5D). Microscopic examination demonstrated that $p18^{-/-}$ mammary cells generated 1.6-fold more luminal colonies (377± 50.3/20,000 cell seeded) than did WT mammary cells (232±30.1/20,000 cell seeded, Figure 5D). $p18^{-/-}$ mammary cells generated slightly more CK5+ cell enriched basal-like colonies (104 ±14.7/20,000 cells seeded) than the WT MECs (87±17.3/20,000 cells seeded), but the increase was not statistically significant (p=0.27, Figure 5D). This result supports a unique function of *p18* in luminal progenitor proliferation and differentiation.

p18 and *GATA3* expression levels are inversely related in human luminal A breast tumors

To determine whether our mouse genetic analysis models human breast cancers, we queried the gene expression data of the Netherlands Cancer Institute 295 (NKI295) breast cancer patient sample set (van de Vijver et al., 2002). The 295 patients were split 50/50 into a “high” and

"low" expression group for each analyzed gene and the distribution of 'high' vs. 'low' expression of each gene was determined relative to five intrinsic tumor subtypes: basal-like, Her2+/ERα−, Luminal A, Luminal B and normal-like as assigned (Fan et al., 2006). Using multiple statistical tests, we determined that *p18* mRNA expression levels were highly correlated with the breast tumor intrinsic subtype (chi-squared $p<0.0001$ (Figure 6A, and Table S2)). Notably, *p18* as well as p19 *INK4D* (data not shown) levels, but not five other CDK inhibitor genes, tended to be low in the Luminal A subtype of human breast cancers ($p = 0.003$), which are almost exclusively ERα+ and high in basal-like tumors ($p <0.0001$). These results are consistent with the finding that mammary tumors developed in $p18^{-/-}$ mice are predominantly comprised of luminal cells and are ERα positive. Interestingly, *RB1* expression is low in basal-like tumors ($p=0.0001$) and high in luminal A tumors ($p=0.0008$) (Figure 6A, and Table S2). An inverse correlation between *p18* and *RB1* expression is consistent with the notion that *p18*, among four *INK4* genes, is the major upstream activator of RB1, and its decrease may relieve selection pressure to decrease or mutate RB1 during tumorigenesis in mammary luminal cells.

GATA3, a member of the GATA family of Zinc finger transcriptional factors, was recently identified to play an essential function in differentiation and maintenance of luminal cell fate and thus for mammary-gland morphogenesis. Restoration of GATA3 in late carcinomas from MMTV-PyMT mice induced tumor differentiation and suppressed tumor dissemination (Kouros-Mehr et al., 2008). Conspicuously, the expression of *GATA3* is high in luminal A and low to absent in basal-like tumors, thus exhibiting an inverse correlation with *p18* (Figure 6A, and Table S2). Scatter plot analysis further confirmed the inverse correlation between *GATA3* and *p18* mRNA levels in human breast cancer patients from the NKI patient series (Correlation coefficient = −0.379, Figure 6B). This finding suggests the possibility of negative regulation of *p18* by GATA3 (see below).

p18 and *GATA3* expression levels predict human breast cancer patient outcomes

We next examined whether the levels of *p18* expression is related to patient outcomes and included all CDK inhibitor genes in the analysis to explore the specificity. Kaplan-Meier analysis of overall survival revealed that "high" vs. "low" expression of $p18^{INK4C}$, $p19^{INK4D}$, and *RB1* genes, but not $p21^{CIP1/WAF1}$, $p27^{KIP1}$, $p57^{KIP2}$, or $p16^{INK4A}$, was significantly predictive of patient outcomes. High *INK4C* and *INK4D* expression and low *RB1* expression predicted poor patient outcome (Figure 6C). Identical results were obtained for relapse-free survival (Figure S5). The statistically significant value of *p18* levels in predicting patient outcome is consistent with, and can be explained by, the correlation between low *p18* expression and luminal A subtype tumors exhibiting a better outcome (Hu et al., 2006). The profiling analyses linking the expression of *INK4* and *RB1* genes with patient outcomes also suggest how an impairment of the RB pathway may clinically predict, and mechanically influence, patient outcomes. A reduction of *RB1* level, among all genes acting on the RB pathway, would be most direct and effective in diminishing the activity of the RB pathway and promoting cell proliferation, and is therefore linked with, or leads to, a more malignant phenotype (i.e. basal-like tumors), while a reduction of its individual upstream activators, such as $p18^{INK4C}$, is less potent in promoting cell division and is linked with less aggressive tumors (luminal A tumors). Notably, contrary to *p18* expression, high *GATA3* expression predicts a better patient outcome, thus showing that human luminal A tumors are characterized by high *GATA3*, high *RB1*, and low *p18*.

GATA-3 negatively regulates *p18* gene expression

Prompted by the inverse correlation between *p18* and *GATA3* expression in human luminal A breast cancer patients, and the recent evidence that *Gata3* is a highly enriched transcription factor in the mammary epithelium of pubertal mice and plays a critical role in luminal cell

differentiation (Asselin-Labat et al., 2007; Kouros-Mehr et al., 2006), we hypothesized that *p18* may be a downstream target of *GATA3* in controlling luminal cell proliferation and differentiation. We first examined the expression of *Gata3* and *p18* in different populations of mammary epithelium. Sorted luminal progenitor enriched $C24^{+}CD29^{-}$ cells from WT mice at a pubertal age (Shackleton, 2006) expressed 12-fold more *Gata3* than $C24^{-}CD29^{-}$ cells that include basal/myoepithelial cells and other cell types (Figure 7A), confirming that *Gata3* is predominantly expressed in luminal epithelium. Interestingly, the *Gata3* mRNA level in MaSC-enriched $C24^{+}CD29^{+}$ cells was also much higher than in $C24^{-}CD29^{-}$ cells, suggesting a potential, and yet to be defined, function of *Gata3* in MaSCs. Again, we observed that the *p18* mRNA level was inversely correlated with *Gata3*; it was significantly lower in both MaSC-enriched $C24^{+}CD29^{+}$ and luminal progenitor enriched $C24^{+}CD29^{-}$ cells than in $C24^{-}CD29^{-}$ cells (Figure 7A).

To directly determine whether Gata3 negatively regulates p18 in mammary epithelium, we first determined the p18 protein level in *Gata3*-deficient mouse mammary tissue. Specific deletion/reduction of *Gata3* in the mammary gland was achieved by pregnancy of *Gata3*$^{f/f}$*;WAP-cre* dams and resulted in a robust increase of p18 protein (Figure 7B). Likewise, the knocking down of *GATA3* expression in human MCF-7 and 293T cells by two different siRNA oligonucleotide duplexes resulted in increased p18 mRNA and protein levels (Figures 7C, 7D). Conversely, overexpression of GATA3 in MCF-10A cells inhibited *p18* mRNA expression (Figure 7E) and increased cell proliferation, as determined by BrdU incorporation (Figure 7F). We also examined *Gata3* expression both in vivo in animals at different ages and in vitro in acini cultured in 3D Matrigel using mammary cells. *Gata3* expression was readily detected, but no discernible difference of *Gata3* expression was detected between the WT and *p18*$^{-/-}$ mammary epithelial cells (data not shown).

Examination of the p18 promoter reveals several GATA3 consensus sites, including a 40-bp region containing 10 GATA3 sequences in tandem located 5.3 kb upstream of the translational initiation ATG codon (Figure 7G). To determine if GATA3 directly binds to the p18 locus, we analyzed 6.6 kb upstream and 2.3 kb downstream of the start codon of the human p18 gene by chromatin-immunoprecipitation (ChIP) assay using 33 pairs of primers. Six out of 33 amplicons, four upstream (a, b, c, and d in Figure 7G) and two downstream of the start codon (h and i in Figure 7G), were specifically enriched in the GATA3 immunoprecipitation (Figure 7G). Except for amplicon h, all positive amplicons contain at least one putative GATA3 binding site (data not shown), including one that contains 10 GATA3 repeats. Together, these results demonstrate that GATA3 binds to the p18 gene and negatively regulates its transcription.

Discussion

Balb/c-*p18* mouse as a model for ER^{+} luminal tumors

In this study, we report that nearly 90% of female *p18* null mice in the Balb/c background spontaneously developed mammary tumors with a median tumor-free survival time of 14 months. To the best of our knowledge, Balb/c-*p18* mice develop mammary tumors at the highest rate among all mutant mice with germline mutations. Our findings support the rate-limiting function of INK4-cyclin Ds-CDK4/6 in suppressing mammary tumorigenesis.

The results presented here also suggest the existence of a genetic modifier(s) in Balb/c mice that interacts with *p18*-deficiency epistatically to promote tumorigenesis. The possibility of p16^{Ink4a}, a tumor suppressor that sustained two allelic variations in Balb/c affecting its inhibitory function toward CDK4 (Zhang et al., 1998), has been ruled out by our observation that *p16*$^{-/-}$;*p18*$^{-/-}$ in CJ57BL/6 background did not develop mammary tumor at an elevated rate (Ramsey et al., 2007). Identifying the modifier(s) remains a daunting challenge, especially

when considering multiple modifiers could have contributed to the tumor susceptibility phenotype in Balb/c.

The mammary tumors developed in Balb/c-*p18* mice are predominantly luminal. In addition to data presented here, gene expression profiling analysis clustered most tumors derived from $p18^{-/-}$ mice with other mice known to have luminal mammary tumors (e.g. MMTV-Neu and MMTV-PyMT) and showed expression of the XBP1 cluster (unpublished results). Our studies demonstrate that loss of *p18* selectively stimulates mammary luminal progenitor cell proliferation at an early age and maintains them at a hyperproliferative state throughout life, leading to increased and sustained proliferation of luminal epithelial cells and eventual development of luminal tumors. Furthermore, the mammary tumors developed in $p18^{-/-}$ mice are ER^+. These features establish the Balb/c-*p18* mouse as an animal model for elucidating the molecular mechanism and cell origin of luminal breast cancers and for preclinical studies of treatment for ER^+ luminal tumors.

Control of luminal cell differentiation by GATA3 and p18

GATA3 is expressed early during embryogenesis and specifically in both ductal and alveolar luminal epithelial cells. Genetic analyses have recently demonstrated that *Gata3* plays multiple morphological and functional roles in mammary development, including terminal end bud, placode and nipple formation, ductal elongation and invasion, and subsequent lactation (Asselin-Labat et al., 2007; Kouros-Mehr et al., 2006). Blockage of luminal progenitor cells to differentiate was recognized as the most likely cellular basis underlying these various functions; the luminal progenitor pool was increased with a concurrent decrease of differentiated luminal cells in MMTV–Cre;$Gata3^{f/f}$ mice, while ectopic expression of *Gata3* in MaSC-enriched cells promoted the stem cells to differentiate along the alveolar cell lineage. Loss of *p18* resulted in expansion of luminal progenitor cells, suggesting that *p18* functions to either restrict stem cells from asymmetric divisions and produce luminal progenitors or to maintain luminal progenitors at a quiescent state (Figure 7H). We further suggest that GATA3 promotes the differentiation of mammary stem cells along the luminal lineage through a network of transcription regulation that, on one hand, represses *p18* expression to allow the expansion of either luminal progenitors or transit cells of luminal lineage and, on the other hand, activates the expression of genes such as *FOXA1* and *ERα* to induce and maintain the differentiation of mature luminal cells. Further investigations are necessary to determine the factor that trans-activates and/or maintains *p18* expression in luminal progenitors.

Loss of *Gata3* would result in an accumulation of *p18* in the luminal progenitor cells, blocking them from entering an active cell cycle and undergoing subsequent differentiation. Loss of *p18*, although stimulating the proliferation of luminal progenitor cells and initiating luminal tumorigenesis, would not significantly impair the differentiation of luminal lineage in the presence of normal GATA3 function. Our study also provides a plausible molecular explanation underlying the pathological association and prognostic feature of GATA3. A high level of GATA3, which has been associated with less aggressive lower grade cancers (Mehra et al., 2005; Sorlie et al., 2003; van de Rijn et al., 2002), would suppress *p18* expression, and a decreased *p18* level would favor the development of luminal type breast cancers that have a better outcome for patients.

p18 and *p16* may collaboratively constrain stem and progenitor cell proliferation

Genetic studies have recently linked the function of *p16* with the control of stem and progenitor cells during aging in neuronal, hematopoietic, and pancreatic lineages (Janzen et al., 2006; Krishnamurthy et al., 2006; Molofsky et al., 2006). These genetic analyses, combined with three lines of evidence from biochemical properties, structural analyses, and the patterns of gene expression, support a model that *p16* and *p18* collaboratively control stem and progenitor

cell cycles. First, rapid turnover of the p21 family of CDK inhibitors and intrinsic stability of INK4 proteins make p21 and INK4 family proteins more suitable for inducing and maintaining a transient and stable cell cycle arrest, respectively. Second, individual INK4 proteins bind to CDK4 and CDK6 with similar affinity. As a result, the activity of CDK4/6 in a given cell is determined by the total concentration of all INK4 combined, rather than individual INK4, making them functionally related and collaborative. Thirdly, *p18* is expressed early and sustains a high level throughout life in many adult tissues, whereas the expression of *p16* is undetectable in young tissues and is induced during aging (Krishnamurthy et al., 2004; Zindy et al., 1997). These observations led us to propose that *p18* and *p16* collaboratively constrain stem cell self-renewal and progenitor cell proliferation, with *p18* playing a major role in maintaining the homeostasis of stem/progenitor cells from early embryogenesis throughout adulthood and *p16* in limiting stem/progenitor cell function during aging.

Experimental Procedures

Mice, histopathology and immunohistochemistry

The generation and genotyping of *p18* and floxed *Gata3* mice have been described previously (Franklin et al., 1998; Pai et al., 2003). *p18* mutant mice in BL/6 background were backcrossed for seven generations with BALB/c mice before used for this study as Balb/c-*p18* mutant mice. Tissues of most organs were removed, fixed in 10% neutral buffered formalin, and examined histologically by two pathologists after H&E staining. Immunohistochemistry and primary antibodies were as described previously (Bai et al., 2003). The IACUC (Institutional Animal Care and Use Committee) at UNC approved all procedures.

Morphologic characterization of mammary epithelium

To examine and quantify small light cell (SLC), undifferentiated large light cell (ULLC), differentiated large light cell (DLLC), large dark cell (LDC), and myoepithelial cell (MYO), we followed criteria defined by Smith and colleagues (Chepko et al., 2005; Smith and Medina, 1988). Cells that could not be clearly defined were categorized as unknown (UK). 3 pairs of WT or $p18^{-/-}$ mice at 2–3 months of age were dissected and stained with H&E. All sections were read by two different pathologists (X-H.P. and B. F.). Only sections containing large amounts of epithelium of sufficient quality for counting were selected. Epithelial structures were classified as ducts when they were singular elements associated with no other epithelial structures. They were classified as lobules if they appeared clustered with other small, round-shaped epithelial structures or if there were small round-shaped structures that budded from a larger, longitudinally sectioned duct. Cells in terminal end buds were also included in the lobule count.

In vivo BrdU labeling assay

For short-term *in vivo* BrdU labeling analysis, mice were injected with 1ml per 100g body weight BrdU cell proliferation labeling reagent (Amersham Bioscience, Little Chalfond, UK) one hour before sacrificing. Tissues were immunostained with anti-BrdU antibody (Abcam, Cambridge, MA). To determine label retaining cells (LRCs), littermate mice at one month of age were injected intraperitoneally with BrdU (50mg/kg) twice a day for seven consecutive days followed by chase for one day or 37 days before sacrificing. 4 μm mammary sections were immunostained with antibodies against BrdU, CK5, and CK8. For counting LRCs, only sections containing a large amount of mammary epithelium of sufficient quality were selected, and only confirmed BrdU positive cells in the duct were counted. Parallel staining of the serial sections for CK8, BrdU, and DAPI was performed to calculate the percentage of $CK8^{+}BrdU^{+}$ cells in $DAPI^{+}$ mammary epithelium.

Four mammary glands (the 4th and 5th pairs) from each mouse were examined, and at least 600 cells per mammary (more than 2400 epithelial cells per mouse) were counted in the parallel staining of serial sections. The average percentages of $BrdU^+$ cells were calculated from three WT and three *p18* null mice, respectively.

Patients and gene-expression data set and statistical analyses

We used a data set of breast-cancer samples from 295 women (van de Vijver et al., 2002). Patients were dichotomized into two groups as above or below median for each gene's expression value (2 based log ratio of red channel intensity and green channel intensity). Kaplan-Meier survival plots were performed for Relapse-Free Survival (RFS) and Overall Survival (OS). Cox-Mantel log-rank tests were applied to compare the survival differences and obtained p-values, using WinSTAT for Excel (R. Fitch Software). We then compared the two groups of patients for each gene versus five breast cancer subtypes(Hu et al., 2006; Sorlie et al., 2003) using two-way contingency-table analyses and SAS software (Cary, NC). All of the statistical analyses were performed with StatsDirect 2.4.3 software (StatsDirect Statistical Software). The survival rate was calculated by the Kaplan-Meier method.

Mammary cell preparation, FACS analysis, Cell sorting, 3D Matrigel assay, Colony-formation assay, Mammosphere assay, Cell culture, Retroviral infection, RNA interference, Western blot, Q-RT-PCR, ChIP assay

Detailed descriptions for these experimental procedures are available in the Supplemental Data.

Supplementary Material

Refer to Web version on PubMed Central for supplementary material.

Acknowledgments

We thank Yojiro Kotake for helping with ChIP assay and Ned Sharpless, Chuxia Deng and Connie Eaves for discussions. F. B. was supported in part by a U.S. Department of Defense Career Postdoctoral fellowship. This study was supported by the NCI Breast SPORE program (P50-CA58223) and the Breast Cancer Research Foundation grants to C.M.P, and an NIH grant (CA68377) to Y.X.

References

Althuis MD, Fergenbaum JH, Garcia-Closas M, Brinton LA, Madigan MP, Sherman ME. Etiology of hormone receptor-defined breast cancer: a systematic review of the literature. Cancer Epidemiol Biomarkers Prev 2004;13:1558–1568. [PubMed: 15466970]

Asselin-Labat ML, Sutherland KD, Barker H, Thomas R, Shackleton M, Forrest NC, Hartley L, Robb L, Grosveld FG, van der Wees J, et al. Gata-3 is an essential regulator of mammary-gland morphogenesis and luminal-cell differentiation. Nat Cell Biol 2007;9:201–209. [PubMed: 17187062]

Bai F, Pei XH, Godfrey VL, Xiong Y. Haploinsufficiency of $p18^{INK4c}$ sensitizes mice to carcinogen-induced tumorigenesis. Mol Cell Biol 2003;23:1269–1277. [PubMed: 12556487]

Bai F, Pei XH, Pandolfi PP, Xiong Y. $p18^{Ink4c}$ and *Pten* constrain a positive regulatory loop between cell growth and cell cycle control. Mol Cell Biol 2006;26:4564–4576. [PubMed: 16738322]

Chang HY, Nuyten DS, Sneddon JB, Hastie T, Tibshirani R, Sorlie T, Dai H, He YD, van't Veer LJ, Bartelink H, et al. Robustness, scalability, and integration of a wound-response gene expression signature in predicting breast cancer survival. Proc Natl Acad Sci USA 2005;102:3738–3743. [PubMed: 15701700]

Chepko G, Slack R, Carbott D, Khan S, Steadman L, Dickson RB. Differential alteration of stem and other cell populations in ducts and lobules of TGFalpha and c-Myc transgenic mouse mammary epithelium. Tissue & cell 2005;37:393–412. [PubMed: 16137731]

Dontu G, Abdallah WM, Foley JM, Jackson KW, Clarke MF, Kawamura MJ, Wicha MS. In vitro propagation and transcriptional profiling of human mammary stem/progenitor cells. Genes & Dev 2003;17:1253–1270. [PubMed: 12756227]

Fan C, Oh DS, Wessels L, Weigelt B, Nuyten DS, Nobel AB, van't Veer LJ, Perou CM. Concordance among gene-expression-based predictors for breast cancer. N Engl J Med 2006;355:560–569. [PubMed: 16899776]

Fantl V, Stamp G, Andrews A, Rosewell I, Dickson C. Mice lacking cyclin D1 are small and show defects in eye and mammary gland development. Genes & Dev 1995;9:2364–2372. [PubMed: 7557388]

Franklin DS, Godfrey VL, Lee H, Kovalev GI, Schoonhoven R, Chen-Kiang S, Su L, Xiong Y. CDK inhibitors $p18^{INK4c}$ and $p27^{KIP1}$ mediate two separate pathways to collaboratively suppress pituitary tumorigenesis. Genes & Dev 1998;12:2899–2911. [PubMed: 9744866]

Herschkowitz JI, Simin K, Weigman VJ, Mikaelian I, Usary J, Hu Z, Rasmussen KE, Jones LP, Assefnia S, Chandrasekharan S, et al. Identification of conserved gene expression features between murine mammary carcinoma models and human breast tumors. Genome Biol 2007;8:R76. [PubMed: 17493263]

Hu Z, Fan C, Oh DS, Marron JS, He X, Qaqish BF, Livasy C, Carey LA, Reynolds E, Dressler L, et al. The molecular portraits of breast tumors are conserved across microarray platforms. BMC Genomics 2006;7:96. [PubMed: 16643655]

Janzen V, Forkert R, Fleming HE, Saito Y, Waring MT, Dombkowski DM, Cheng T, DePinho RA, Sharpless NE, Scadden DT. Stem-cell ageing modified by the cyclin-dependent kinase inhibitor p16INK4a. Nature 2006;443:421–426. [PubMed: 16957735]

Kouros-Mehr H, Bechis SK, Slorach EM, Littlepage LE, Egeblad M, Ewald AJ, Pai SY, Ho IC, Werb Z. GATA-3 links tumor differentiation and dissemination in a luminal breast cancer model. Cancer Cell 2008;13:141–152. [PubMed: 18242514]

Kouros-Mehr H, Slorach EM, Sternlicht MD, Werb Z. GATA-3 maintains the differentiation of the luminal cell fate in the mammary gland. Cell 2006;127:1041–1055. [PubMed: 17129787]

Krishnamurthy J, Ramsey MR, Ligon KL, Torrice C, Koh A, Bonner-Weir S, Sharpless NE. p16INK4a induces an age-dependent decline in islet regenerative potential. Nature 2006;443:453–457. [PubMed: 16957737]

Krishnamurthy J, Torrice C, Ramsey MR, Kovalev GI, Al-Regaiey K, Su L, Sharpless NE. Ink4a/Arf expression is a biomarker of aging. J Clin Invest 2004;114:1299–1307. [PubMed: 15520862]

Latres E, Malumbres M, Sotillo R, Martin J, Ortega S, Martin-Caballero J, Flores JM, Cordon-Cardo C, Barbacid M. Limited overlapping roles of $p15^{INK4b}$ and $p18^{INK4c}$ cell cycle inhibitors in proliferation and tumorigenesis. EMBO J 2000;19:3496–3506. [PubMed: 10880462]

Mehra R, Varambally S, Ding L, Shen R, Sabel MS, Ghosh D, Chinnaiyan AM, Kleer CG. Identification of GATA3 as a breast cancer prognostic marker by global gene expression meta-analysis. Cancer Res 2005;65:11259–11264. [PubMed: 16357129]

Molofsky AV, Slutsky SG, Joseph NM, He S, Pardal R, Krishnamurthy J, Sharpless NE, Morrison SJ. Increasing $p16^{INK4a}$ expression decreases forebrain progenitors and neurogenesis during ageing. Nature 2006;443:448–452. [PubMed: 16957738]

Ormandy CJ, Musgrove EA, Hui R, Daly RJ, Sutherland RL. Cyclin D1, EMS1 and 11q13 amplification in breast cancer. Breast Cancer Res Treat 2003;78:323–335. [PubMed: 12755491]

Pai SY, Truitt ML, Ting CN, Leiden JM, Glimcher LH, Ho IC. Critical roles for transcription factor GATA-3 in thymocyte development. Immunity 2003;19:863–875. [PubMed: 14670303]

Pei XH, Bai F, Smith MD, Xiong Y. $p18^{Ink4c}$ collaborates with Men1 to constrain lung stem cell expansion and suppress non-small-cell lung cancers. Cancer Res 2007;67:3162–3170. [PubMed: 17409423]

Perou CM, Sorlie T, Eisen MB, van de Rijn M, Jeffrey SS, Rees CA, Pollack JR, Ross DT, Johnsen H, Akslen LA, et al. Molecular portraits of human breast tumours. Nature 2000;406:747–752. [PubMed: 10963602]

Ponnaiya B, Cornforth MN, Ullrich RL. Radiation-induced chromosomal instability in BALB/c and C57BL/6 mice: the difference is as clear as black and white. Radiat Res 1997;147:121–125. [PubMed: 9008202]

Ramsey MR, Krishnamurthy J, Pei XH, Torrice C, Lin W, Carrasco DR, Ligon KL, Xiong Y, Sharpless NE. Expression of $p16^{Ink4a}$ compensates for $p18^{Ink4c}$ loss in cyclin-dependent kinase 4/6-dependent tumors and tissues. Cancer Res 2007;67:4732–4741. [PubMed: 17510401]

Schmitz NM, Leibundgut K, Hirt A. MCM4 shares homology to a replication/DNA-binding domain in CTF and is contacted by pRb. Biochem Biophys Res Comm 2004;317:779–786. [PubMed: 15081408]

Shackleton M, Vaillant F, Simpson KJ, Stingl J, Smyth GK, Asselin-Labat ML, Wu L, Lindeman GJ, Visvader JE. Generation of a functional mammary gland from a single stem cell. Nature 2006;439:84–88. [PubMed: 16397499]

Sherr CJ. Cancer cell cycle. Science 1996;274:1672–1677. [PubMed: 8939849]

Sicinski P, Donaher JL, Parker SB, Li T, Fazeli A, Gardner H, Haslam SZ, Bronson RT, Elledge SJ, Weinberg RA. Cyclin D1 provides a link between development and oncogenesis in the retina and breast. Cell 1995;82:621–630. [PubMed: 7664341]

Sleeman KE, Kendrick H, Ashworth A, Isacke CM, Smalley MJ. CD24 staining of mouse mammary gland cells defines luminal epithelial, myoepithelial/basal and non-epithelial cells. Breast Cancer Res 2006;8:R7. [PubMed: 16417656]

Sleeman KE, Kendrick H, Robertson D, Isacke CM, Ashworth A, Smalley MJ. Dissociation of estrogen receptor expression and in vivo stem cell activity in the mammary gland. J Cell Biol 2007;176:19–26. [PubMed: 17190790]

Smith GH. Label-retaining epithelial cells in mouse mammary gland divide asymmetrically and retain their template DNA strands. Development 2005;132:681–687. [PubMed: 15647322]

Smith GH, Medina D. A morphologically distinct candidate for an epithelial stem cell in mouse mammary gland. J Cell Sci 1988;90:173–183. [PubMed: 3198708]

Sorlie T, Tibshirani R, Parker J, Hastie T, Marron JS, Nobel A, Deng S, Johnsen H, Pesich R, Geisler S, et al. Repeated observation of breast tumor subtypes in independent gene expression data sets. Proc Natl Acad Sci USA 2003;100:8418–8423. [PubMed: 12829800]

Stingl J, Eaves CJ, Zandieh I, Emerman JT. Characterization of bipotent mammary epithelial progenitor cells in normal adult human breast tissue. Breast Cancer Res Treatment 2001;67:93–109.

Stingl J, Eirew P, Ricketson I, Shackleton M, Vaillant F, Choi D, Li HI, Eaves CJ. Purification and unique properties of mammary epithelial stem cells. Nature 2006;439:993–997. [PubMed: 16395311]

Ullrich RL, Bowles ND, Satterfield LC, Davis CM. Strain-dependent susceptibility to radiation-induced mammary cancer is a result of differences in epithelial cell sensitivity to transformation. Radiat Res 1996;146:353–355. [PubMed: 8752316]

Uziel T, Zindy F, Xie S, Lee Y, Forget A, Magdaleno S, Rehg JE, Calabrese C, Solecki D, Eberhart CG, et al. The tumor suppressors Ink4c and p53 collaborate independently with Patched to suppress medulloblastoma formation. Genes & Dev 2005;19:2656–2667. [PubMed: 16260494]

van de Rijn M, Perou CM, Tibshirani R, Haas P, Kallioniemi O, Kononen J, Torhorst J, Sauter G, Zuber M, Kochli OR, et al. Expression of cytokeratins 17 and 5 identifies a group of breast carcinomas with poor clinical outcome. Am J Pathol 2002;161:1991–1996. [PubMed: 12466114]

van de Vijver MJ, He YD, van't Veer LJ, Dai H, Hart AA, Voskuil DW, Schreiber GJ, Peterse JL, Roberts C, Marton MJ, et al. A gene-expression signature as a predictor of survival in breast cancer. N Engl J Med 2002;347:1999–2009. [PubMed: 12490681]

Wang TC, Cardiff RD, Zukerberg L, Lees E, Arnold A, Schmidt EV. Mammary hyperplasia and carcinoma in MMTV-cyclin D1 transgenic mice. Nature 1994;369:669–671. [PubMed: 8208295]

Welm BE, Tepera SB, Venezia T, Graubert TA, Rosen JM, Goodell MA. Sca-1(pos) cells in the mouse mammary gland represent an enriched progenitor cell population. Dev Biol 2002;245:42–56. [PubMed: 11969254]

Yu Q, Geng Y, Sicinski P. Specific protection against breast cancers by cyclin D1 ablation. Nature 2001;411:1017–1021. [PubMed: 11429595]

Yu Q, Sicinska E, Geng Y, Ahnstrom M, Zagozdzon A, Kong Y, Gardner H, Kiyokawa H, Harris LN, Stal O, et al. Requirement for CDK4 kinase function in breast cancer. Cancer Cell 2006;9:23–32. [PubMed: 16413469]

Zarkowska T, U S, Harlow E, Mittnacht S. Monoclonal antibodies specific for underphosphorylated retinoblastoma protein identify a cell cycle regulated phosphorylation site targeted by CDKs. Oncogene 1997;14:249–254. [PubMed: 9010227]

Zhang S, Ramsay ES, Mock BA. Cdkn2a, the cyclin-dependent kinase inhibitor encoding $p16^{INK4a}$ and $p19^{ARF}$, is a candidate for the plasmacytoma susceptibility locus, Pctr1. Proc Natl Acad Sci USA 1998;95:2429–2434. [PubMed: 9482902]

Zindy F, Quelle DE, Roussel MF, Sherr CJ. Expression of the $p16^{INK4a}$ tumor suppressor versus other INK4 family members during mouse development and aging. Oncogene 1997;15:203–211. [PubMed: 9244355]

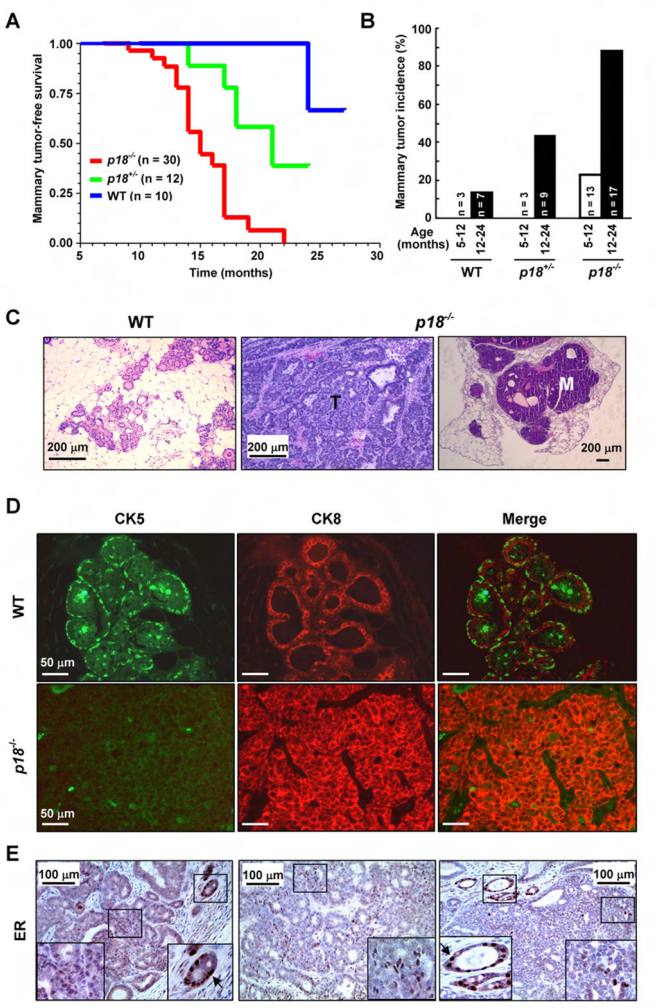

Figure 1.

p18 null mice develop spontaneous luminal mammary tumors

(A) Mammary tumor-free survival of Balb/c mice of different genotypes.

(B) Spontaneous tumor development in Balb/c-*p18* mutant mice.

(C) Representative H&E staining of primary mammary tumor (T) and lung metastasis (M) developed in $p18^{-/-}$ mice. A WT mammary control at a similar age is shown.

(D) Immunofluorescent staining of CK5 and CK8 in age-matched (14–16 months of age) mammary tissue from WT mice or tumors from mutant mice. Note that the patched green signals inside the WT glands were autofluorescence caused by the secretion of milk.

(E) Immunohistochemical staining of ERα (brown) in mammary tumors from $p18^{-/-}$ mice. Note the highly expressed ERα levels in normal mammary glands (arrows) surrounding tumors. Boxed areas are magnified in the insets.

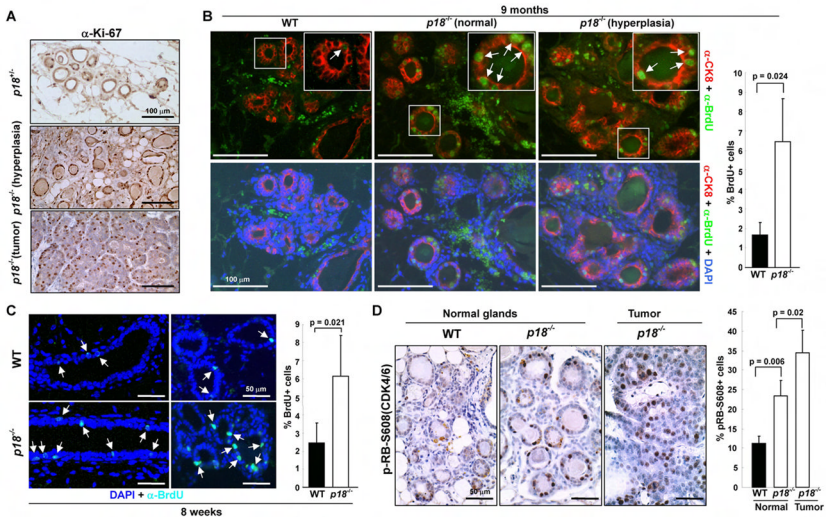

Figure 2.

Increased cell proliferation and Rb protein phosphorylation in *p18*$^{-/-}$ mammary epithelium and tumors

(A) Immunostaining of Ki67 (brown) of 18-month old virgin *p18*$^{+/-}$ and *p18*$^{-/-}$ mammary glands.

(B) Immunostaining of BrdU (green), CK8 (red), and DAPI (blue) in mammary glands of 9-month-old virgin littermate mice. The boxed areas were enlarged in the insets to show BrdU incorporation (pointed by white arrows) in an individual gland. The percentages of BrdU positive cells were calculated from cells situated in clear duct/gland structure. Results represent the mean ± SD of 3 animals per group.

(C) Immunostaining of BrdU (green) in mammary glands of 8-week-old virgin littermate mice was performed to determine cell proliferation and nuclei were stained with DAPI (blue). The percentages of BrdU positive cells were calculated from cells situated in clear duct/gland structure. Results represent the mean ± SD of 3 animals per group.

(D) Sections of normal mammary glands and mammary tumors of WT and *p18*$^{-/-}$ mice at around one year of age were examined for pRb protein phosphorylation at Ser608 by CDK4 and CDK6. Counter staining is blue and positive staining is brown. The percentages of pRb-S608 positive cells were calculated from cells situated in clear duct/gland structure in normal glands and from all cells in tumors. Results represent the mean ± SD of 3 animals per group.

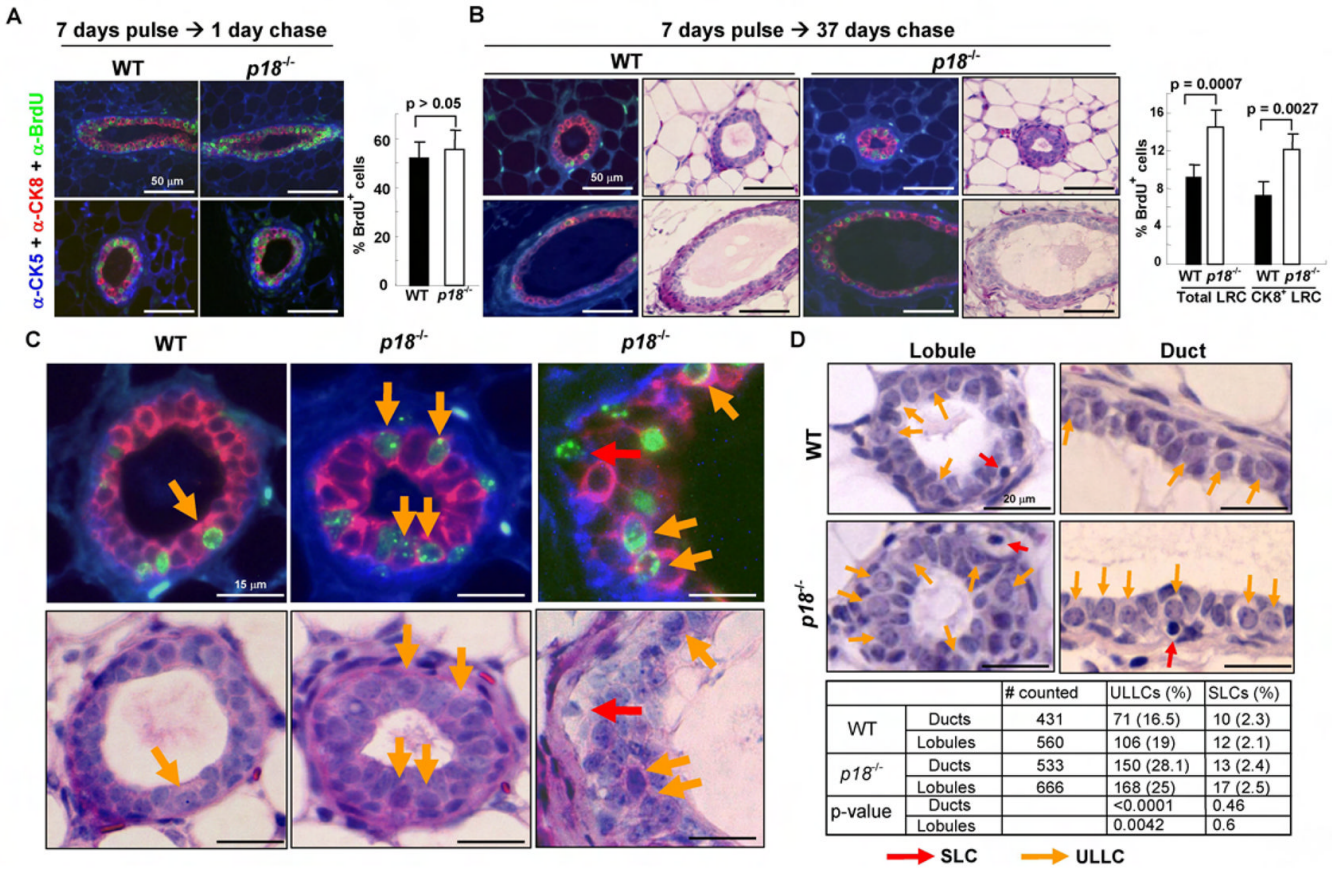

		# counted	ULLCs (%)	SLCs (%)
WT	Ducts	431	71 (16.5)	10 (2.3)
	Lobules	560	106 (19)	12 (2.1)
p18$^{-/-}$	Ducts	533	150 (28.1)	13 (2.4)
	Lobules	666	168 (25)	17 (2.5)
p-value	Ducts		<0.0001	0.46
	Lobules		0.0042	0.6

Figure 3.

Loss of *p18* increases label-retaining luminal epithelial cells and cells with morphologic features of luminal progenitors

(A) and (B) 1-month-old littermate mice were injected intraperitoneally with BrdU twice a day for seven consecutive days, followed by chase for one (A) or 37 days (B) before sacrifice. Mammaries were dissected and stained with antibodies to BrdU, CK5, and CK8. The percentage of BrdU positive cells were calculated as described in the Experimental Procedures. Results represent the mean ± SD of 3 animals per group.

(C) After immunofluorescence staining and photographing of sections from the label retaining assay (37 days chase, top panels), the identical section was re-stained with H&E. Matched cells between two stainings were identified microscopically and label-retaining small light cells (SLCs) and undifferentiated large light cells (ULLCs) were counted (indicated by red and yellow arrows, respectively, bottom panels). Lower magnification pictures for these paired stainings were also shown in (B). Three additional types of histological distinct cell types—differentiated large light cells (DLLCs), large dark cells (LDCs), and myoepithelial cells (MYOs)—were also identified and quantified (see Table S1).

(D) Littermate WT or *p18*$^{-/-}$ mice at 2–3 months of age were dissected and stained with H&E. SLCs and ULLCs are indicated by red and yellow arrows, respectively. 400–600 ductal and lobular cells from each genotype were counted, and the number and percentage of SLCs and ULLCs are presented. Three other histological types (DLLCs, LDCs, and MYOs) were also identified and quantified (Figure S1).

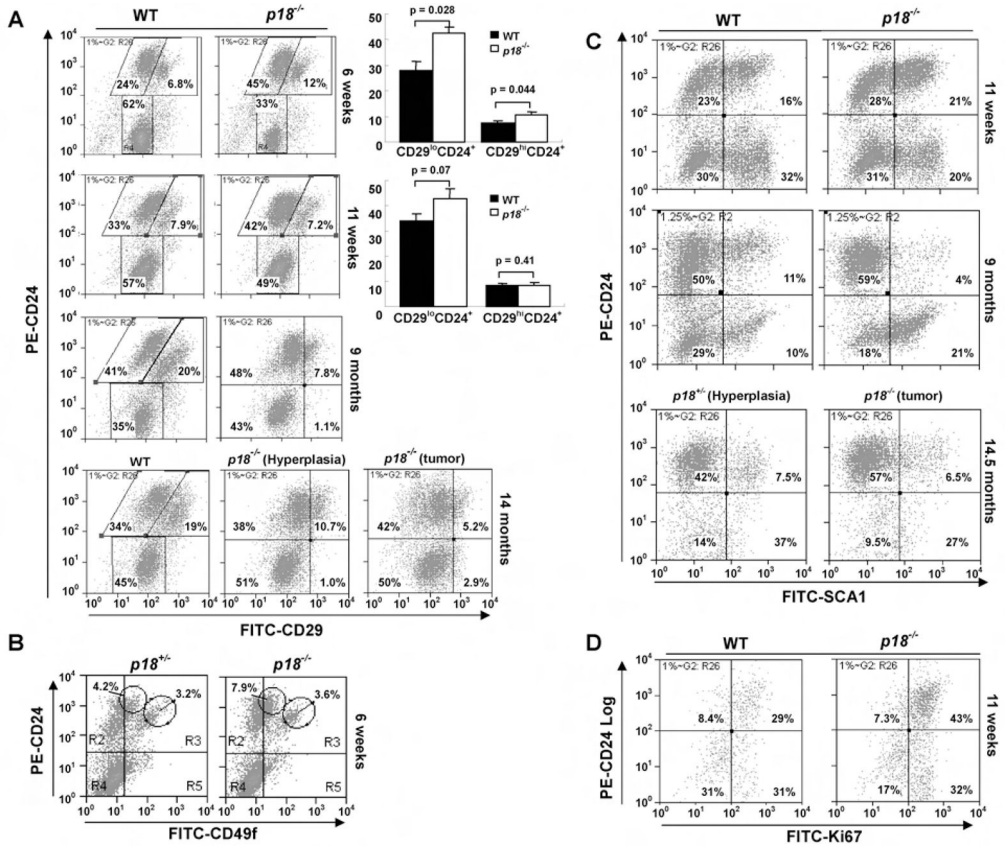

Figure 4.

p18 loss expands luminal progenitors

(A, B, C, D). Mammary cells from WT (or $p18^{+/-}$) and $p18^{-/-}$ virgin littermate mice of Balb/c backgrounds at indicated ages were isolated, sorted, and analyzed by flow cytometry for CD24 together with CD29 (A); CD49f (B); SCA1 (C), or Ki67 (D). The bar graphs in (A) represent the mean ± SD of 3 animals per group.

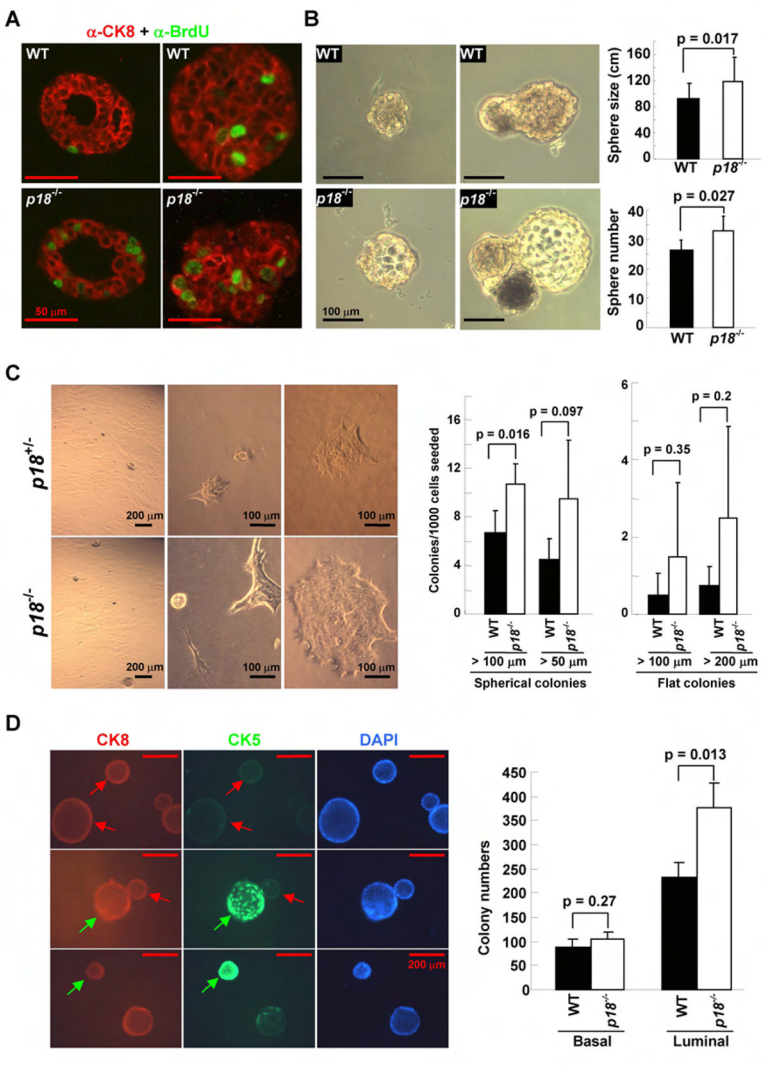

Figure 5.

p18 deficiency increases luminal progenitor cell proliferation in vitro

(A) Mammary cells freshly isolated from both WT and $p18^{-/-}$ mice were cultured in 3D Matrigel for one week, pulse labeled with BrdU, and acini were stained for antibodies to CK8 (red) and to BrdU (green). Two sections from two separate acini are shown.

(B) Mammary cells from WT and $p18^{-/-}$ virgin littermate mice at 2–3 months of age were isolated and analyzed by mammosphere assay. Representative mammospheres in common size (left panel) and in large size (right panel) are shown. The sphere size was measured as described in the Supplemental Experimental Procedures, and the number of spheres larger than 60 μm was quantified. The assay was performed in triplicate for each animal. The bar graphs represent the mean ± SD of 4 animals per group.

(C) Freshly isolated mammary cells were plated in Matrigel-coated 24-well plate (1,000 cells per well). Nine days after culture, colonies were photographed and counted. Representative spherical and flat colonies are shown. The assay was performed in triplicate for each animal. The bar graphs represent the mean ± SD of 3 animals per group.

(D) Freshly isolated mammary cells were plated in Matrigel-coated 24-well plate (20,000 cells per well). Nine days after culture, colonies were stained with CK8 and CK5 on Matrigel and counted as described in the Supplemental Experimental Procedures. Representative luminal

(red arrows) and myoepithelial colonies (green arrows) are indicated. The assay was performed in triplicate for each animal. The bar graphs represent the mean ± SD of 3 animals per group.

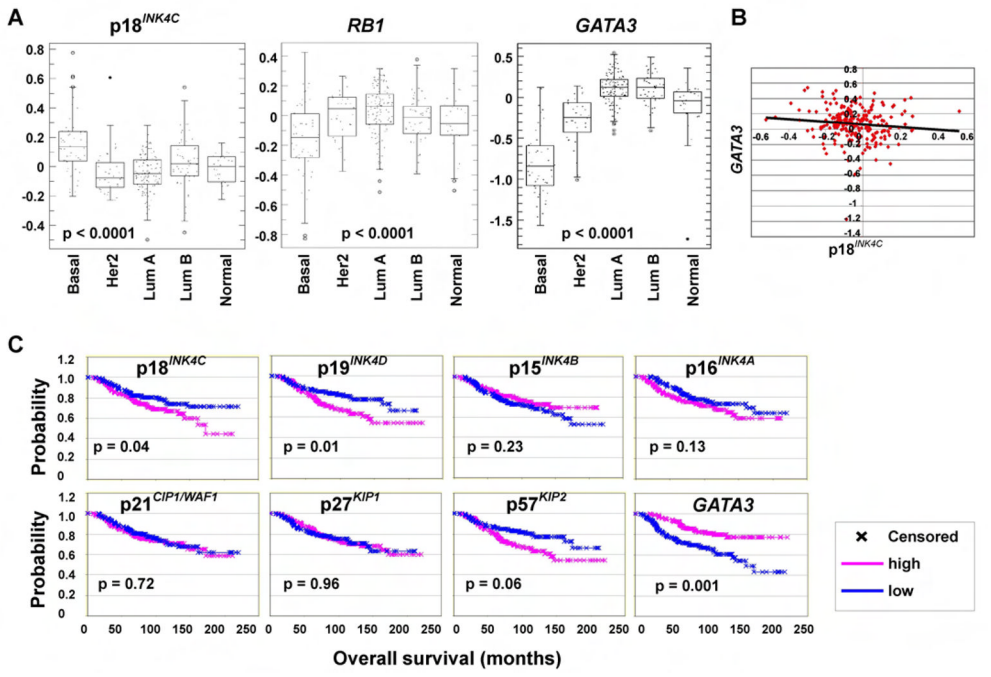

Figure 6.

p18 and GATA3 level is inversely related to luminal A type tumors and conversely predicts human breast cancer patient outcomes

(A) ANOVA and box plot analysis of gene expression levels in 295 breast cancer patients from the NKI patient series (Chang et al., 2005; van de Vijver et al., 2002) according to tumor subtype.

(B) Scatter plot analysis of *INK4C* and *GATA3* expression for 295 patients from the NKI patient series. Correlation coefficient (r) = −0.379, p value<0.0001.

(C) 295 patients from the NKI patient series were divided into high and low groups based upon each gene's rank order expression values. Probabilities for overall survival are shown for each gene and the *p* values calculated.

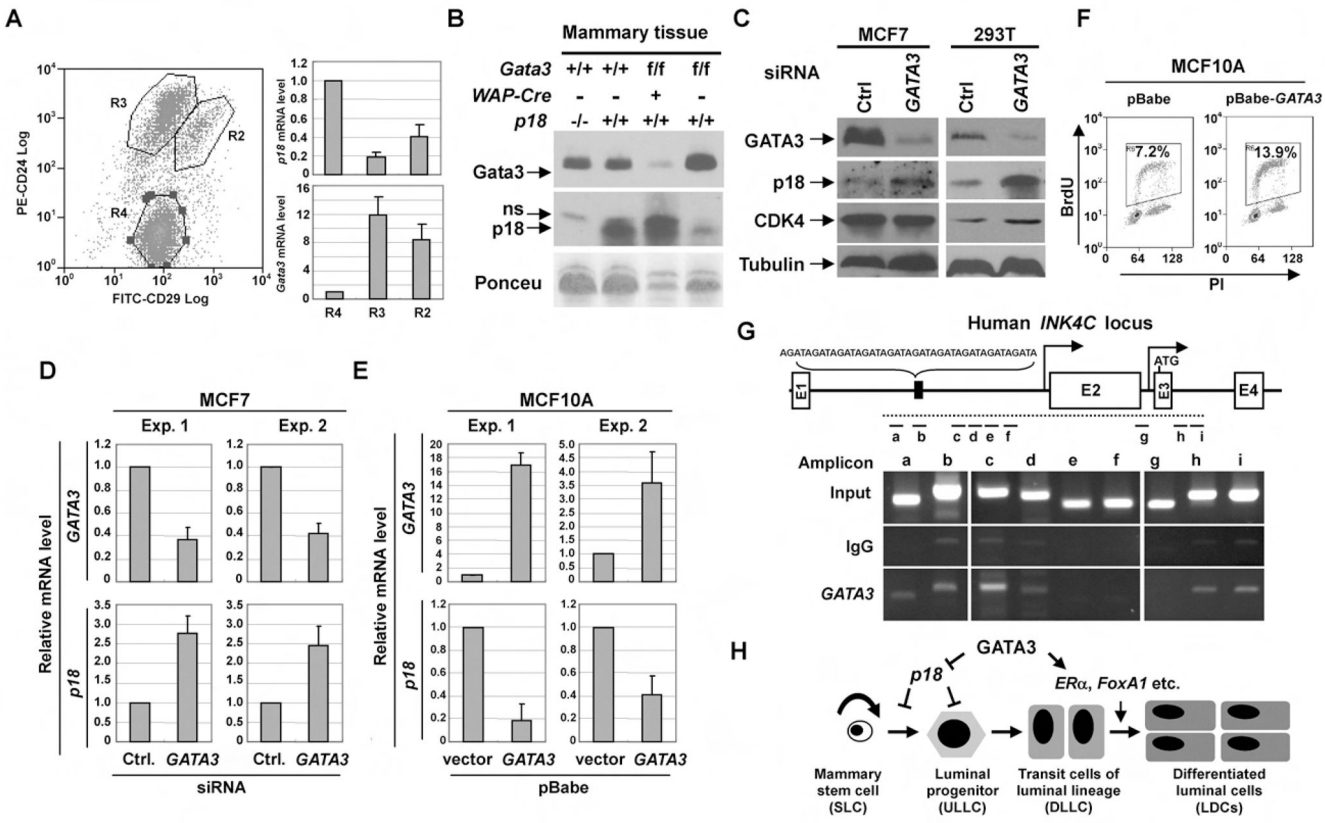

Figure 7.

p18 is a direct target of GATA3 in mammary epithelium.

(A) Mammary cells from WT mice at seven weeks of age were isolated and sorted by flow cytometry for CD24 and CD29 cell populations. Total RNA from the indicated cell populations (R4, $CD24^{-}CD29^{-}$; R3, $CD24^{+}CD29^{-}$; R2, $CD24^{+}CD29^{+}$) was extracted and analyzed for the expression of *Gata3* and *p18* by Q-RT-PCR. Data are expressed relative to the corresponding values for R4 populations as mean ± SD from triplicates of each of the two independent mice.

(B) Mammary tissues from *Gata3*$^{f/f}$;WAP-cre^{+} and *Gata3*$^{f/f}$;WAP-cre^{-} dams that successfully produced and nursed pups were analyzed for *Gata3* and *p18* expression. Mammary tissues from 2-month old virgin WT and *p18* null females were used as control. n.s., non-specific bands.

(C, D) Human MCF-7 or 293T cells were transfected with either scrambled siRNA (Ctrl) or siRNA targeting *GATA3*, and the cells were lysed for Western blot, (C) or the RNA were extracted for Q-RT-PCR (D) 48 hours after transfection. Similar results were derived from two different siRNA targeting different sequences of *GATA3*. Data are expressed relative to the corresponding values for control (Ctrl) cells as mean ± SD from triplicates of a representative experiment.

(E) MCF-10A cells were infected with pBabe-puro or pBabe-puro-GATA3, selected with puromycin for two to five days, and analyzed by Q-RT-PCR. Data are expressed relative to the corresponding values for vector-infected cells as mean ± SD from triplicates of a representative experiment.

(F) MCF-10A cells infected with pBabe-puro-empty or pBabe-puro-GATA3 were pulse-labeled with BrdU. Cells were stained with anti-BrdU antibody and PI and subjected to flow cytometry. BrdU positive cells are marked by the box and the percentage of BrdU positive cells are shown.

(G) GATA3 binds to *p18* locus. The upper panel illustrates the human *p18* locus which expresses multiple transcripts, including a longer 2.4-kb transcript from an upstream promoter and a shorter 1.2-kb transcript from a downstream promoter. A 40 bp region containing 10 GATA sequences in tandem is shown. The dotted line represents the 8.9 kb region screened for GATA3 binding by ChIP assay using 33 pairs of primers. Locations and results of representative amplicons are shown, MCF-7 cells were used for this assay.
(H) Working model for the function and mechanism of *GATA3* and *INK4c* in regulating mammary stem, progenitor, and luminal cell differentiation.